PORT SAID ENGINEERING RESEARCH JOURNAL

Faculty of Engineering - Port Said University
Volume 29 No. 1 pp: 20:32

Finite Element Investigation of Composite Cold-Formed Steel Beam with Concrete Slab

Ashraf Elsabbagh[1], Mohamed Abdellatif[2], Mohamed Elghandour[3], Tarek Sharaf[4]*

[1] *Associate professor, Civil Engineering Department, Faculty of Engineering, Port Said University, Port Said, Egypt, Email: ashref.ismail@eng.psu.edu.eg*

[2] *Ph.D. Candidate, Department of Civil Engineering, Higher Institute of Engineering and Technology, Arish, Egypt, Email: engmsol55@gmail.com*

[3] *Professor, Civil Engineering Department, Faculty of Engineering, Port Said University, Port Said, Egypt, E-mail: dr.elghandor@gmail.com*

[4] *Associate professor, Civil Engineering Department, Faculty of Engineering, Port Said University, Port Said, Egypt, Email: tarek.sharaf@eng.psu.edu.eg*

**Corresponding author, DOI: 10.21608/PSERJ.2024.314285.1361*

Received 10-9-2024
Revised 24-9-2024
Accepted 25-9-2024

ABSTRACT

The structural performance of a T-Composite CFS Beam and a Concrete Slab was investigated using Finite Element Analysis. In this study, eight experimental composite beam specimens were validated, and ninety-six Finite Element models were evaluated under flexure. Three cross-section shapes (T, Y, and R) were studied. All parts have a monosymmetric steel cross section that connects to a 1000 mm wide concrete slab. The current study seeks to evaluate various cross-section modifications, such as cold formed steel (CFS) form, beam depth, flange width, slab thickness, and beam span. All models were tested using four-point loading and simple support conditions. The section failure modes and load capacity of all specimens were determined using finite element analysis (FEA) data. It has been observed that the verified models' results have a very good agreement. Additionally, the new parametric study results showed that the Y-shape is better than the R-shape and T-shape because of the presence of the filled top flange, which causes more stiffness for the section and increases the section load-carrying capacity by 28% more than the T-shape. Changing parameters such as increasing slab thickness enhances the section load capacity by about 42%, 9% for changing beam width, and 51% for increasing beam depth.

Keywords: Finite element analysis, Composite beams, Cold-formed sections, Steel-concrete composite sections.

1. INTRODUCTION

Recently, composite constructions have gained popularity and are to a large measure responsible for the strength of steel frames in many countries. Composite beams are frequently used due to advantages such as weight savings, greater rigidity, faster erection, longer spans, and construction benefits [1-2]. The (CFS) is generally employed in low-rise buildings, commercial structures, and the construction sector. Typically, the CFS section thickness varied from 1.2 mm to 3.2 mm. [3]. However, because of its slenderness, the CFS is susceptible to failure modes are local buckling, lateral-torsional buckling, and lateral distortional buckling [4]. The use of composite action might improve the CFS section's response to instability concerns. The CFS section is attached to the concrete slab using suitable shear connections or friction between the embedded components in the concrete. This connection causes tension in the CFS element, while the concrete slab is compressed. Hanaor [5] examined the composite effects caused by concrete and CFS I-sections. Lawson et al. [6] were the first to describe composite beams made out of twin cold-formed steel sections, a concrete slab, and a shear connection or propelled strip. Liu and Lakkavalli [7] examined the strength of concrete and CFS C-section composite slab joists under four shear transfer conditions: surface bonding, self-drilling screws, prefabricated bent-up tabs, and predrilled holes. Irwan et al. [8-9] described a unique transfer improvement called as the Bent-up Triangular Tab, which uses small triangular tabs bent to the desired angle and formed on the upper face of the CFS section. Ahmed Kamar et al. [10] examined the variables affecting the distribution of

stress and the sliding of concrete slabs inside composite beams. T.M. Alhajri, M. M Tahir, et al. [11] investigated the performance of a pre-cast U-shaped composite beam formed by fusing a ferro-cement slab with CFS. Y.C. Wong examined partial shear interaction detection in composite steel-concrete beams [12]. Ashraf M. Abou-Rayan et al. [13] Examine the flexural behavior of a CFS I-beam with reinforced hollow tube flanges through an experimental investigation. Richard, J.Y., et al.'s study [14] examines into how fatigue and static loads affect composite beams. All investigators concluded that concrete slabs and CFS sections might interact compositely. However, statistics and information on the behavior and performance of CFS in composite construction remain unclear. Several factors can impact composite slab behavior when hybrid CFS beams are used, including design, span, stiffener usage, form, and CFS section thickness. As a result, this study describes and evaluates a novel composite slab made up of hybrid CFS beams embedded in CFS flooring using the ABAQUS FEA tool. To resist buckling, it is made up of a built system, cold-formed steel sections, and a slab that interacts compositely through friction between the cold-formed beams' embedded components and the slab. This method of manufacture may give an alternate composite material for the flooring and roofs of medium and small-sized constructions. Slabs are thin reinforced concrete elements made up of many layers of fine wire mesh or small diameter rods evenly disseminated throughout the composite matrix to strengthen concrete [15-17]. In addition to being an appropriate material for CFS structure building, stiffeners for CFS beams may increase their performance [18-19].

2. FINITE ELEMENT MODELLING

2.1. General

Finite element analysis was performed using ABAQUS to model the concrete slab's behavior with the composite CFS beams. The initial geometric imperfections loading conditions, supporting conditions, geometric characteristics, and mechanical characteristics were all taken into account. We observed and examined the moment-displacement curves, ultimate strengths, and failure mechanisms for these sections.

2.2. Finite Element Meshing.

The mesh density used to simulate the model determines how accurate the FEA results are. It is appropriate to increase the element numbers in the mesh to improve the accuracy. To find the most accurate mesh size, a sensitivity analysis was performed. While the truss element (T3D2) represented the steel wire mesh, the solid element (C3D8R) was used to duplicate the CFS beams with the concrete slab (see to Fig. 1). Figure 2 illustrates three sizes of mesh for T-4000-NS: fine mesh 10x10 mm^2, medium mesh 25x25 mm^2, and coarse mesh 50x50 mm^2, while Figure 3 illustrates the T-4000-NS analysis results. Because the results for the three types were very similar, a medium-sized mesh of 25x25 mm^2 was chosen to reduce run time while maintaining the necessary accuracy for analysis.

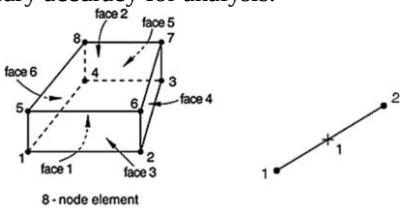

Figure 1: Types of elements used in simulation.

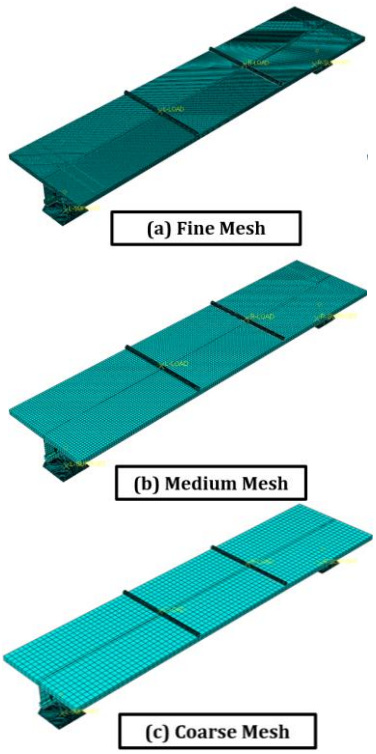

Figure 2: Fine, medium, and coarse meshes.

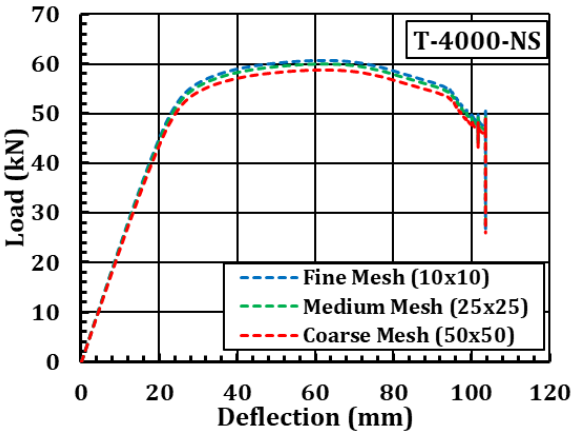

Figure 3: Mesh sensitivity analysis for T-4000-NS

2.3. Material Simulation

2.3.1. CF Steel

Figure 4a illustrates the elastic-plastic curve utilized for predicting CFS material parameters while accounting for hardening behavior [20–22]. The strain range of the horizontal yielding branch is 1–10 times the elastic strain (ε_y). It is assumed that the ultimate strain (ε_u) is 0.2. The material statistics were obtained as follows: elastic modulus E = 206 GPa, yield strength f_y = 330 MPa, and ultimate strength fu = 430 MPa. The steel plates have a Poisson ratio of 0.3.

2.3.2. Concrete

A concrete damage plasticity model has been used to characterize the nonlinear behavior of the concrete slab. The basic equations in [23–24] were used to represent nonlinear compressive and tensile interactions. The dilation angle Ψ=30◦, flow potential eccentricity =0.1, strength ratio fb_0/fc_0=1.16 between biaxially and uniaxially compressed concrete, invariable stress ratio K_c=0.667, and viscosity parameter μ=0.0 are the five factors taken into account when defining a CDP model in ABAQUS. The concrete's stress-strain failure is shown in Figure 4b.

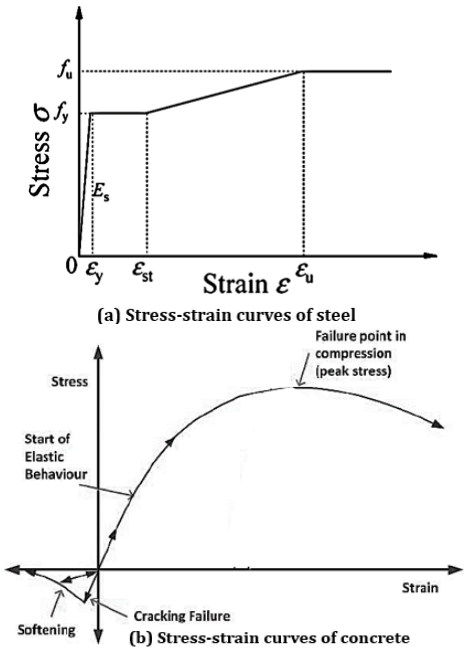

(a) Stress-strain curves of steel

(b) Stress-strain curves of concrete

Figure 4: Stress-strain curve for steel and concrete.

2.4. Load Simulation and Boundary Conditions

Every FEA model was tested under simple support conditions with four-point loading. Static general analysis in ABAQUS was utilized regularly, with the Newton-Raphson solution approach. Simulated FE models were utilized to replicate the boundary and loading conditions found in the test procedures reported by T. Sharaf et al. [25]. Figure 5 shows the boundary and load conditions for the FE models. Figure 5 shows controlled displacements in all directions of the two end-bearing supports. To maintain model stability, longitudinal displacement (UX) at midspan joints was controlled in the X direction. The vertical displacement of the joints under load was regulated in order to model displacement loading and carry out a displacement control analysis. To evaluate the beam's loading capacity, the response at the supports was employed.

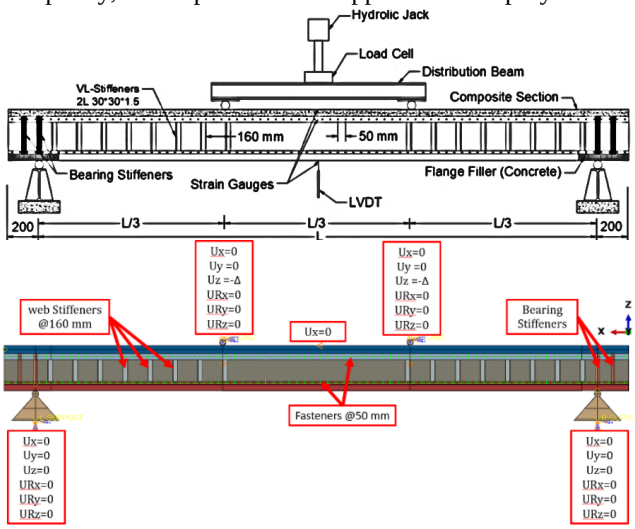

Figure 5: Load and boundary conditions for FE models with stiffeners [25].

2.5. Fastener and contact condition.

Fastener characteristics were developed such that all rotational and translational degrees of freedom of the nodes were bound at the bolt point. To simulate bolts, ABAQUS fastener functions were employed, with a bolt diameter of 6 mm. Contact was examined between the flanges and the web, the lower flange with the support, and the rollers of loading with the slab. As a tie contact, surface-to-surface contact with finite sliding was utilized, with "hard" contact pressure provided to represent their interaction. The contact is termed penalty friction, with a friction value of 0.3. The concrete slab acts as the host, and the embedded contact joins the steel wire mesh and the upper part of the top flange to it. Figure 6 illustrates the locations of bolts and touched surfaces.

2.6. Geometrical Imperfections

The FE study of composite CFS beams took into account the effects of geometrical imperfections. Schafer and Pekoz [26] indicate that the equation used to determine the value of the initial imperfections in the FEA is ($d_1 \approx 6t^{-2}$). Geometrical imperfections in the FE analysis have been taken into consideration by doing an elastic buckling analysis. The most significant buckling mode indicated the geometric imperfections that existed originally. As a result, the second mode in the current analysis is found to be the worst buckling mode out of the first ten, which is chosen for this study. One can obtain the geometric update ratio by using equation (1). The buckling mode seen in Figures 7-9 is thought to be the worst possible mode for T-, Y- and R-beams.

$$G.update ratio = \left(\frac{initial\ imperfection\ value}{maximum\ deformation\ value} \right) \quad (1)$$

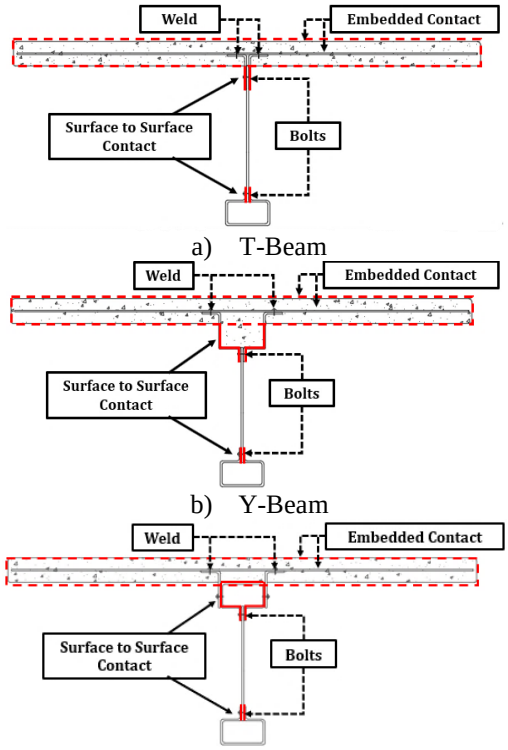

Figure 6: Location of bolts and contact surfaces.

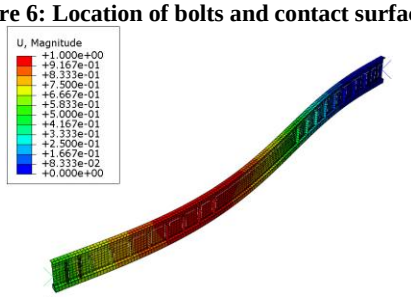

Figure 7: Buckling modes for T-4000-WS beams.

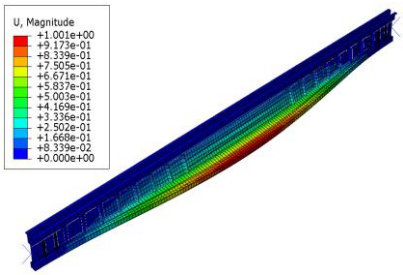

Figure 8: Buckling modes for Y-4000-WS beams.

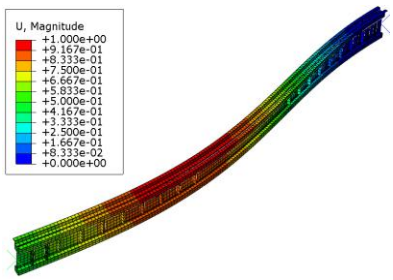

Figure 9: Buckling modes for R-4000-WS beams.

2.7. Residual Stresses

Residual stresses on the cross-section are formed during the cold-forming process of steel sections, causing steel plates to yield quickly. In CFS structural members, two types of residual stresses exist: bending residual stresses and membrane residual stresses. Wan and Mahendran [27] after investigating the impacts of residual stresses on CFS beams, it was shown that these stresses had no bearing on the ultimate loads. Consequently, the effect of residual stress on CFS beams was not taken into account in the current investigation.

3. Verification of The Finite Element Model

3.1. General

FE analysis was used to verify the eight experimentally tested specimens. Four models represented T-shaped beams, while four represented Y-shaped beams. The models featured two stiffening conditions: no stiffeners and stiffeners placed 160mm apart at the shear zone. Two alternative beam lengths (4000 mm and 5000 mm) were investigated. The beam configurations and cross sections are given in Table 1 and Figure 10.

Table 1: Tested beam configurations for two lengths 4000 mm and 5000 mm [25] (all dimensions in mm).

Model	Steel Cross-Section Dimensions						RC Slab Dimensions and Reinforcement	
	h_f	b_f	h_L	t_f	t_w	d		
T-NS T-WS Y-NS Y-WS	40	50	20	1.5	1.2	270	1000 × 50	Wire Mesh 30×30 mm $\phi = 3mm$ $F_y = 360MPa$

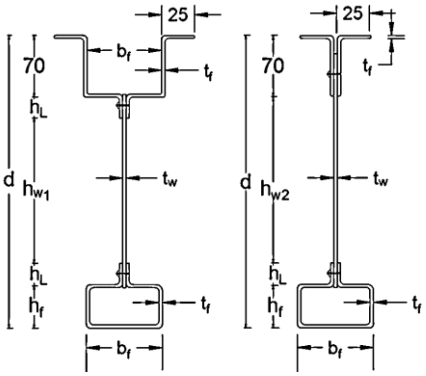

Figure 10: Cross-section dimensions for Y and T beams [25].

3.2. Verifications of Results

The vertical deflection curves indicate the beam's midspan deflection. Figures 11-18 illustrate the verified load versus deflection, load versus strain, and failure processes for T and Y beams. The data show that the FEA and experimental results are very comparable.

3.3. Verifications of Failure Modes

Figures 11-18 provide a comparison of failure modes obtained by FEA and experimental testing [25]. The

most frequent failure modes in CFS beams are lateral buckling and local buckling, both of which are impacted by the thinness of the steel. Figures 11-18 show how local buckling develops in the web following lateral buckling. The use of FEA to parametrically examine the behavior of a composite CFS beam with changing section dimensions is supported by a comparison of experimental and FEA results using load-strain curves, failure modes, and load-deflection curves.

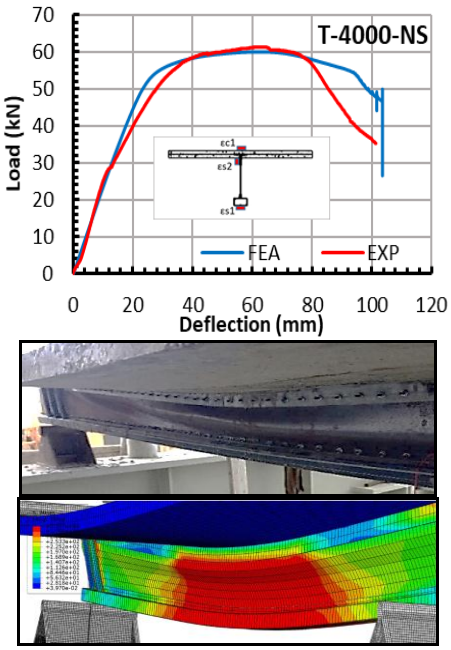

Figure 11: Comparison between EXP and FEA results for T-4000-NS.

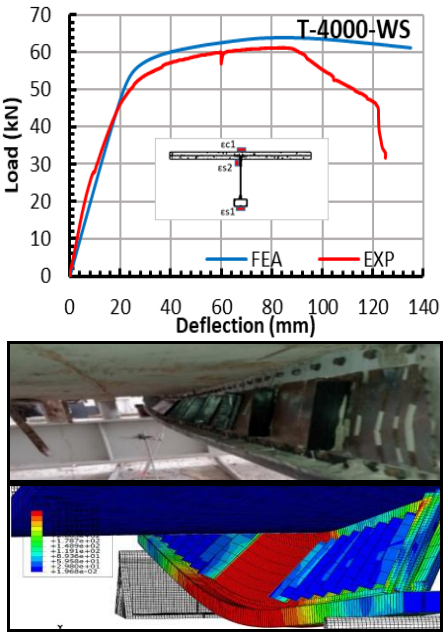

Figure 12: Comparison between EXP and FEA results for T-4000-WS.

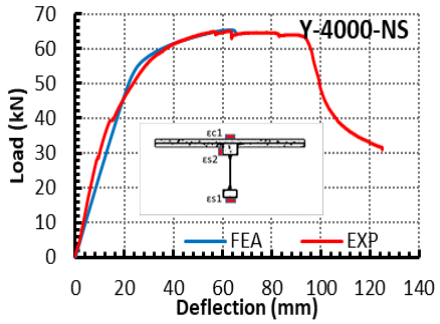

Figure 13: Comparison between EXP and FEA results for Y-4000-NS.

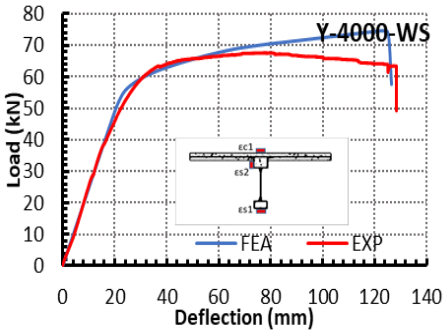

Figure 14: Comparison between EXP and FEA results for Y-4000-WS.

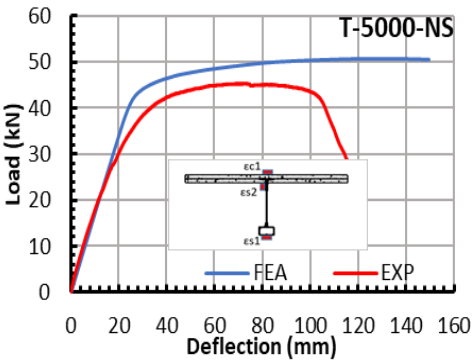

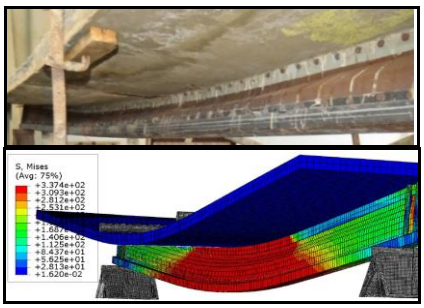

Figure 15: Comparison between EXP and FEA results for T-5000-NS.

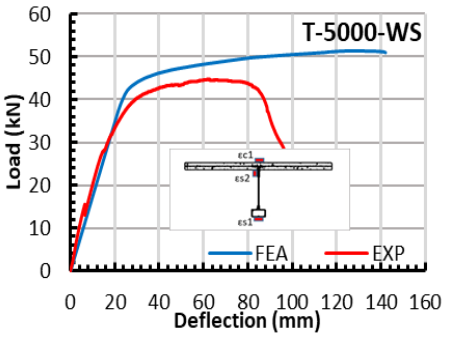

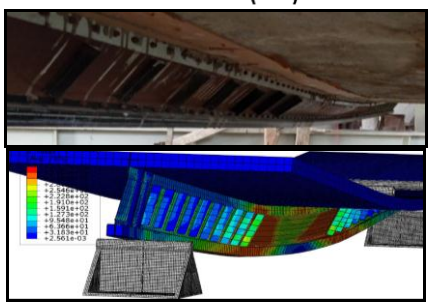

Figure 16: Comparison between EXP and FEA results for T-5000-WS.

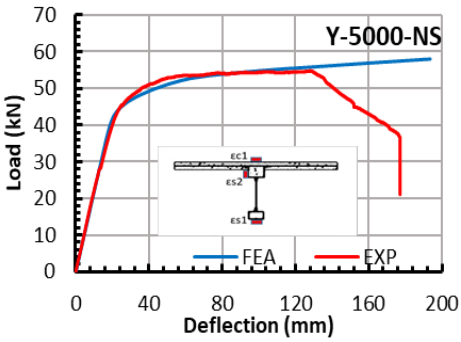

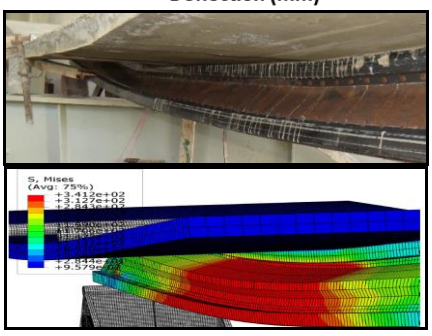

Figure 17: Comparison between EXP and FEA results for Y-5000-NS.

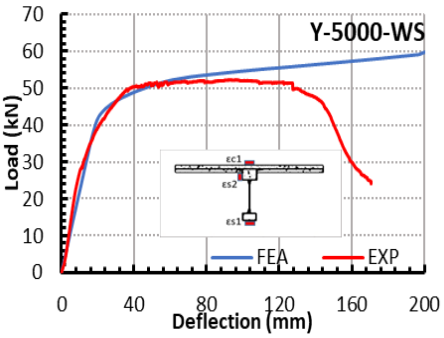

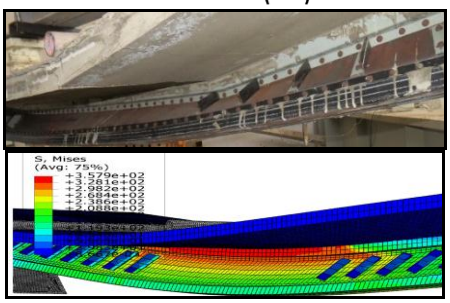

Figure 18: Comparison between EXP and FEA results for Y-5000-WS.

4. Parametric Study

Create a new database on the composite beam and concrete slab by doing parametric research using the validated model findings. The 96 models utilized in this study have T-beam, Y-beam, and R-beam cross sections. Each cross-section has two beam depths (270mm and 370mm), two slab thicknesses (50mm and 70mm), two steel thickness cases ($t_w<t_f$ and $t_w>t_f$), two flange widths (50mm and 60mm), and two beam lengths (5000mm and 4000mm). According to T.Sharaf et al.'s experimental findings [25], the new parametric investigation should sustain the stiffening condition. Table 2 shows the beam configurations for T, Y, and R beams, whereas Figure 19 shows the cross-sections of typical beams.

Table 2: Parametric study configurations for T, Y, and R-shape with two spans of 4000mm and 5000mm (all dimensions in mm).

Beam	RC Slab			CFS Beam Dimensions					
	B	t_s	Reinforcement	*d*	t_w	b_f	t_f	h_f	h_L
B-WS-1	1000	50		270	1.2	50	1.5	40	20
B-WS-2	1000	70		270	1.2	50	1.5	40	20
B-WS-3	1000	50		270	1.5	50	1.2	40	20
B-WS-4	1000	70		270	1.5	50	1.2	40	20
B-WS-5	1000	50		270	1.2	60	1.5	40	20
B-WS-6	1000	70	Wire Mesh	270	1.2	60	1.5	40	20
B-WS-7	1000	50	Size	270	1.5	60	1.2	40	20
B-WS-8	1000	70	30×30 mm	270	1.5	60	1.2	40	20
B-WS-9	1000	50	Single Layer	370	1.2	50	1.5	40	20
B-WS-10	1000	70	ϕ=3mm	370	1.2	50	1.5	40	20
B-WS-11	1000	50	Fy=360 Mpa	370	1.5	50	1.2	40	20
B-WS-12	1000	70		370	1.5	50	1.2	40	20
B-WS-13	1000	50		370	1.2	60	1.5	40	20
B-WS-14	1000	70		370	1.2	60	1.5	40	20
B-WS-15	1000	50		370	1.5	60	1.2	40	20
B-WS-16	1000	70		370	1.5	60	1.2	40	20

B = T, Y and R-shapes

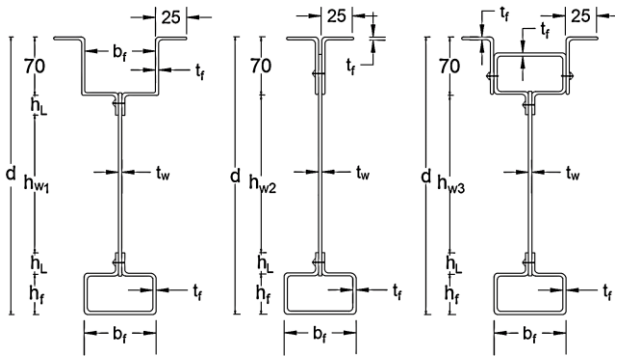

Figure 19: Cross-section dimensions for Y, T, and R beams.

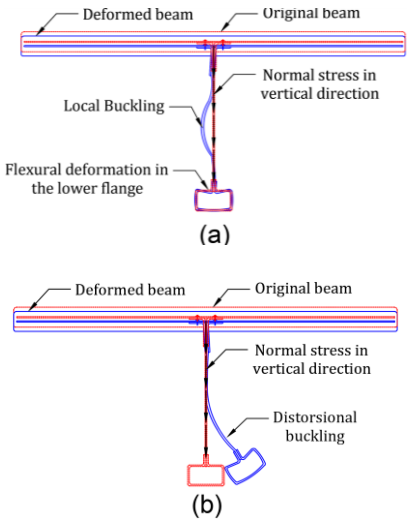

Figure 20: T-beam deformed shapes [25].

4.1. Parametric Study Results

Table 3 lists the FEA total load (P_u) values at the ultimate case for T, Y, and R beams with spans 4000mm and 5000mm, and also represents the vertical deflections (in mm) at ultimate load (in kN) for each beam model.

Table 3: FEA results.

Beam	T-WS				Y-WS				R-WS			
	4000 mm		5000 mm		4000 mm		5000 mm		4000 mm		5000 mm	
	P_u	δ_u	P_u	δ_u	P_u	δ_u	P_u	δ_u	P_u	δ_u	P_u	δ_u
1	74.0	162	54.8	203	94.4	299	63.9	301	84.6	181	59.1	231
2	104.5	202	71.4	212	122.3	227	86.3	301	112.8	202	73.6	208
3	71.5	175	54.0	213	88.3	293	59.3	289	75.9	167	56.0	190
4	100.2	222	68.7	224	120.2	299	81.7	300	108.0	240	71.0	180
5	80.7	231	57.9	203	99.8	235	67.3	292	86.2	255	61.8	200
6	108.7	154	74.1	202	127.4	223	90.9	299	120.2	220	76.5	208
7	74.4	158	56.1	221	91.6	274	62.4	284	80.2	172	59.6	196
8	100.8	187	69.8	230	124.1	259	83.8	280	113.7	250	73.3	209
9	108.9	107	81.8	174	129.4	157	93.1	263	118.3	230	86.9	221
10	125.7	113	100.8	196	154.6	166	115.2	258	143.1	169	104.5	213
11	107.5	151	77.2	218	128.0	197	88.6	231	114.5	266	80.1	199
12	123.6	151	93.7	223	151.1	192	108.8	228	140.1	288	95.0	202
13	112.1	105	87.1	202	130.8	168	98.0	251	120.5	171	90.6	230
14	136.8	143	108.3	203	163.2	166	120.4	250	153.4	183	108.8	214
15	110.4	144	83.1	160	130.0	172	93.5	241	117.8	262	87.3	214
16	131.7	128	96.0	150	156.3	166	115.6	246	150.7	262	101.4	188

4.2. Failure Modes

Increasing the load causes a slab cracks. By further increasing the load, the lower flange's catenary overall effect and the impact of the web normal stresses in the vertical direction, the lower flange was deformed under localized flexural stresses as shown in Figure 20 Subsequently, the web experiences two types of buckling: distortional buckling, which is similar to unbraced column buckling close to the beam failure, and local buckling at relatively low load levels. Vertical compressive loads induce distortion buckling, which results in the web bowing out of plane, overcoming the lateral stiffness of the lower flange and causing the steel beam to twist as it fails. Figures 21-22 illustrate examples of failure modes for composite CFS beams with depths of 270mm and 370mm and slab thicknesses of 50mm and 70mm, respectively where L_t=4000 mm.

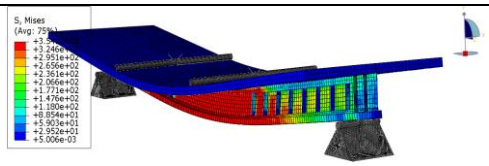

(a) T-WS-1

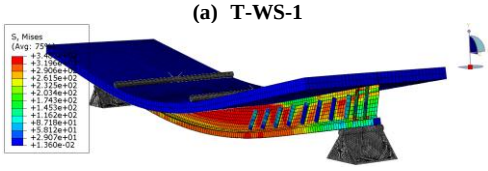

(b) T-WS-2

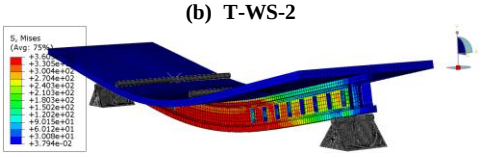

(c) Y-WS-1

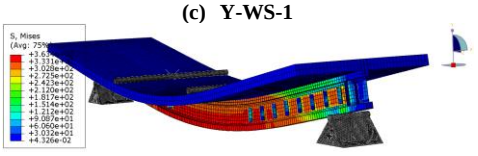

(d) Y-WS-2

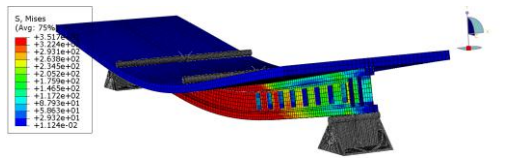

(e) R-WS-1

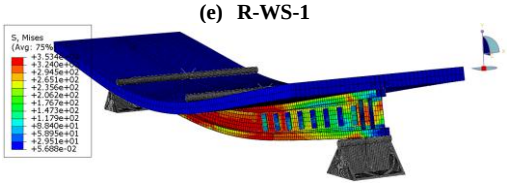

(f) R-WS-2

(g)

Figure 21: FEA failure mode for 4000 mm beams with a depth of 270mm and slab thicknesses of 50mm, and 70mm.

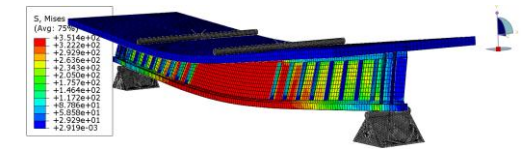

(a) T-WS-9

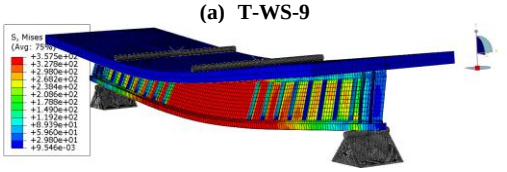

(b) T-WS-10

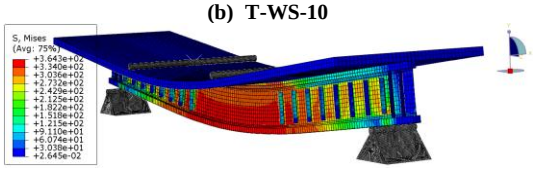

(c) Y-WS-9

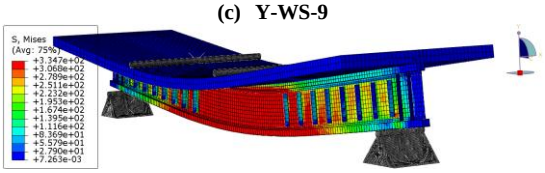

(d) Y-WS-10

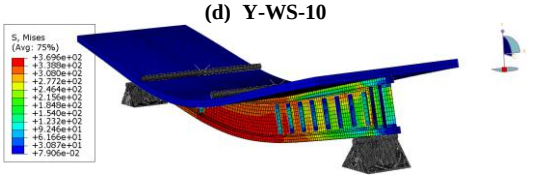

(e) R-WS-9

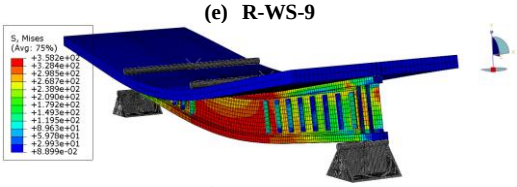

(f) R-WS-10

Figure 22: FEA failure mode for 4000 mm beams with a depth of 370mm and slab thicknesses of 50mm, and 70mm.

4.3. Effect of Cross-Section Shape

The beams' stiffness and load-bearing capabilities are the result of their cross-sectional form. The results in Table 3 showed that the Y-beams had the maximum section load capacity, followed by the R-beams and T-beams. Figure 23 shows the percentage difference between T, Y, and R beams with spans of 4000mm and 5000mm. The section load capacity of Y-4000 beams rises by approximately 28%, 14% for R-4000 beams, 23% for Y-5000 beams, and 9% for R-5000 beams, exceeding that of T-beams. Y-beams may outperform R and T-beams due to the filled top flange, which boosts the section's rigidity. R-beams are less sectionally load capacity due to the presence of the upper hollow flange, which cripples due to the normal stress concentration in the web direction; however, the existence of the upper flange decreases the web height (h_w), which could mitigate the local buckling in the web; for this reason, the T-beams have the lower degree in section load capacity.

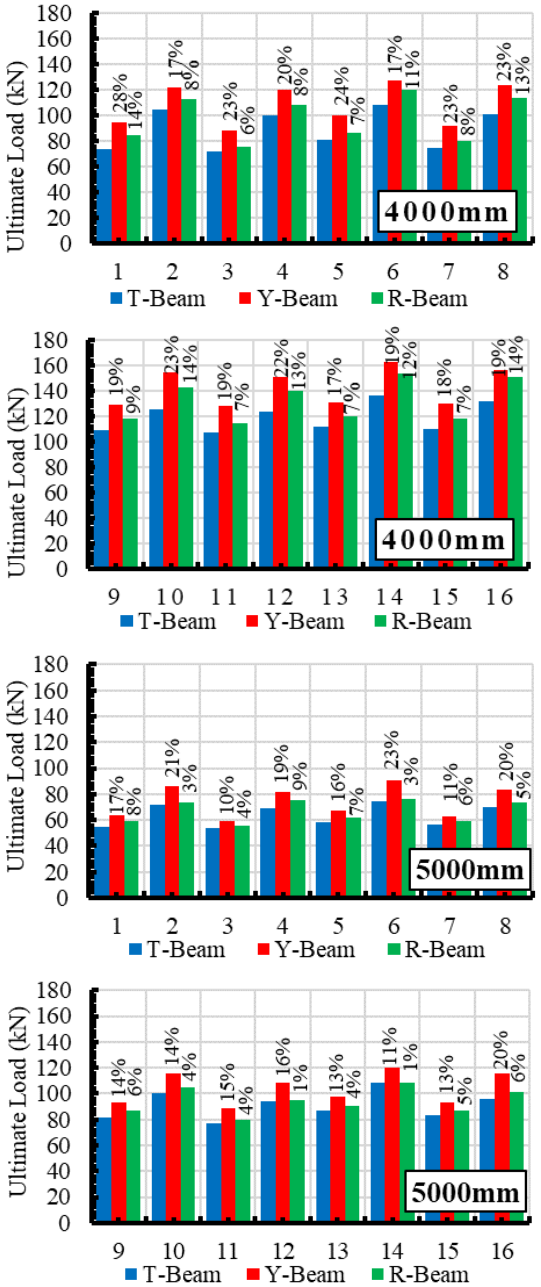

Figure 23: Comparison between the results for T, Y and R beams with spans 4m and 5m

4.4. Effect of the changing in steel thicknesses

Figure 24 illustrates the difference in section load capacity for beams with ($t_w<t_f$ and $t_w>t_f$). As illustrated in Figure 24, the findings reveal that using a larger web thickness than the flange thickness reduces section load capacity by approximately 8% for T-4000, 8% for Y-4000, 10% for R-4000, 11% for T-5000, 8% for Y-5000, and 9% for R-5000 beams. It was found that in all of the models, the section load capacity improved by choosing a flange thickness larger than the web thickness.

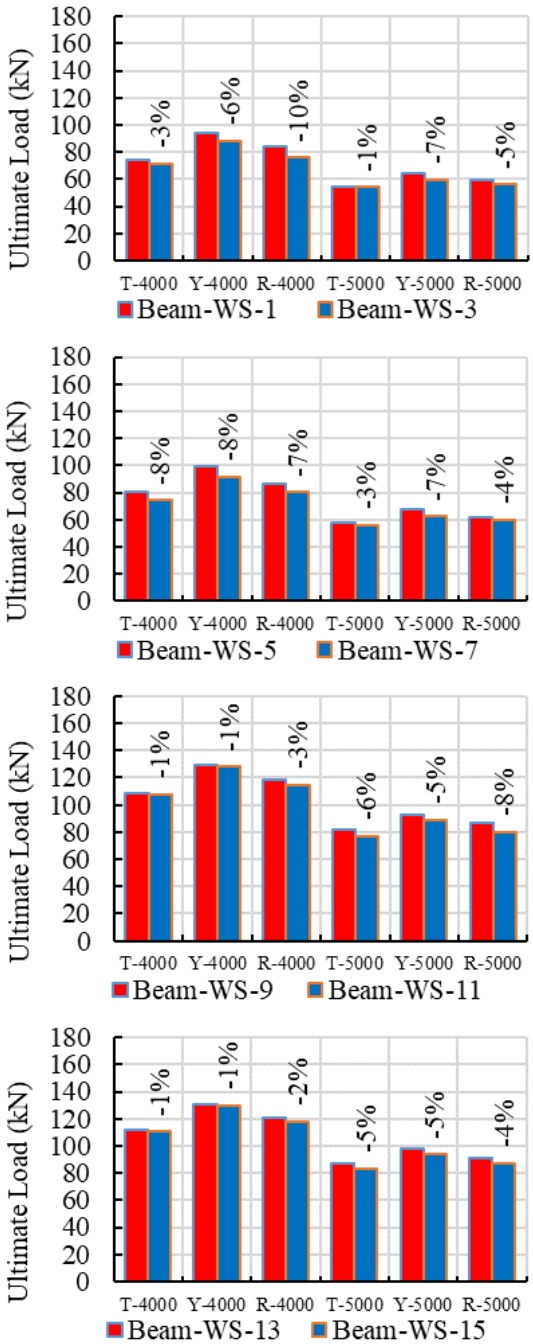

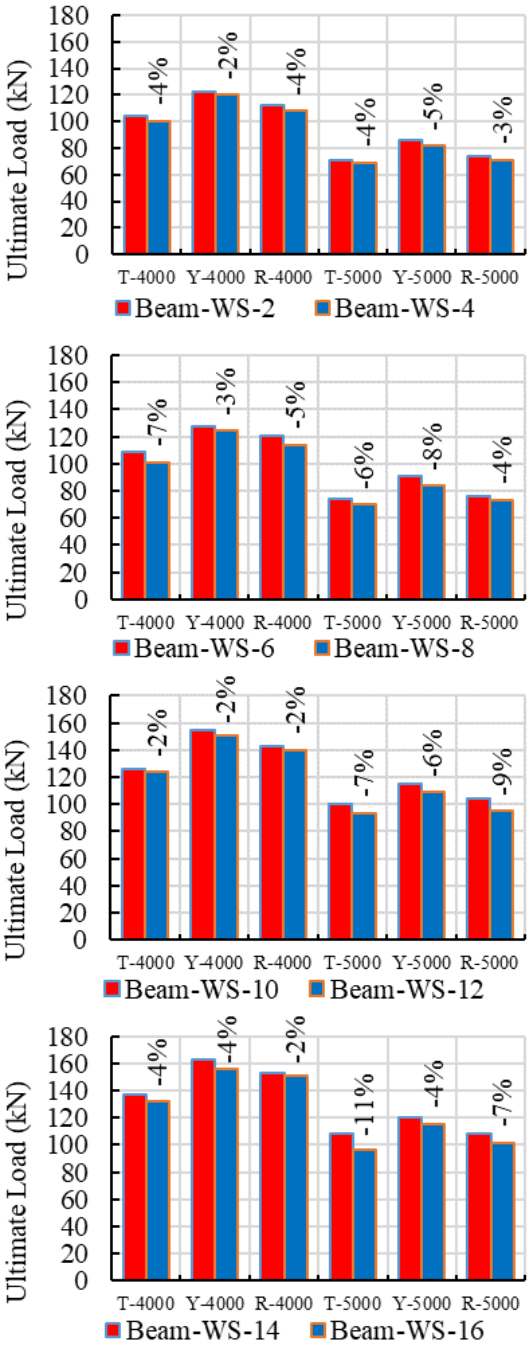

Figure 24: Difference in section load capacity for the beams with ($t_w<t_f$ and $t_w>t_f$).

4.5. Effect of the change in slab thickness

Figure 25 represents the difference in section load capacity for beams with slab thicknesses of 50mm and 70mm. It is found that the increase in slab thickness increases the ultimate load capacity by about 41%, 36%, and 42% for T-4000, Y-4000, and R-4000-beams respectively, and increases by 30% for T-5000mm and 38% for Y-and 27% for R-5000-beams.

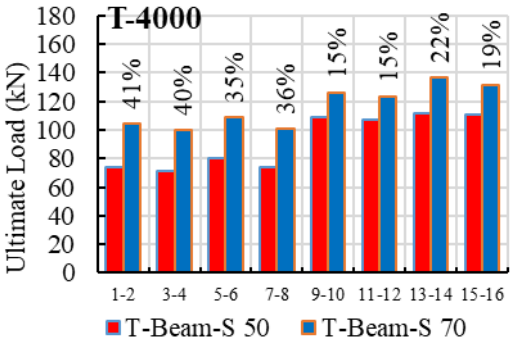

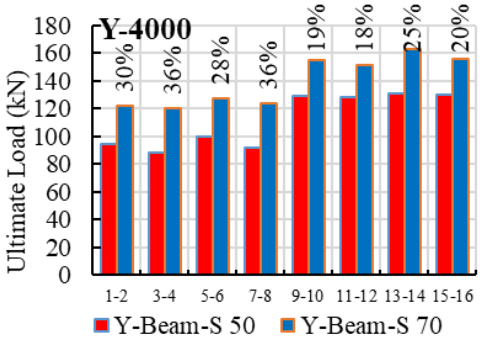

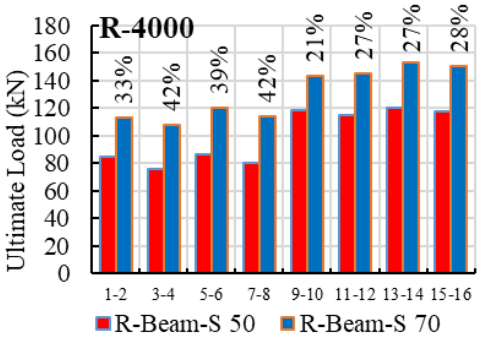

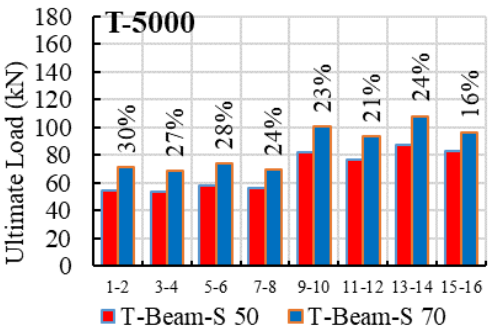

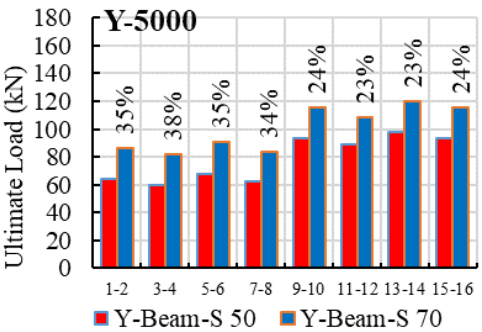

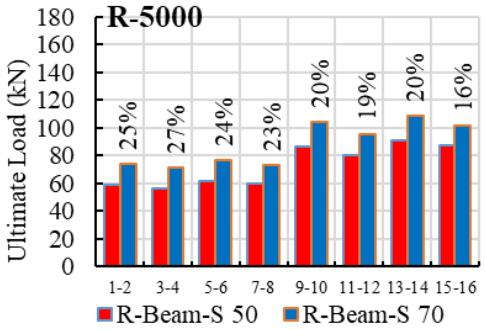

Figure 25: Difference in section load capacity for slab thicknesses 50mm and 70mm.

4.6. Effect of changing steel beam width

Increasing the flange width causes a slight increase in the ultimate load of the beams, the effect of using a larger flange width for the beams with a span of 4000mm doesn't exceed 9% for T-beams, 6% for Y-beams, and 7% for R-beams, and for beams with a span of 5000mm doesn't exceed 7%, 6% and 9% for T, Y, and R beams respectively. Figure 26 illustrates the comparison between the beams with 50mm and 60mm in width.

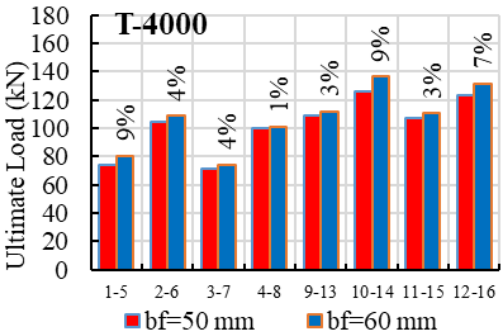

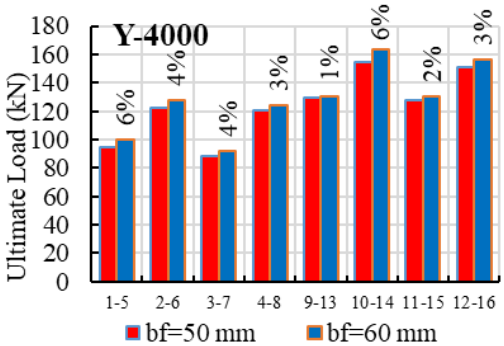

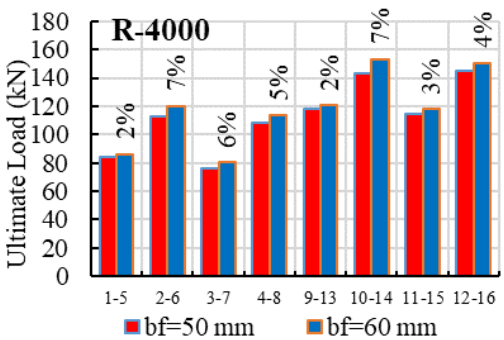

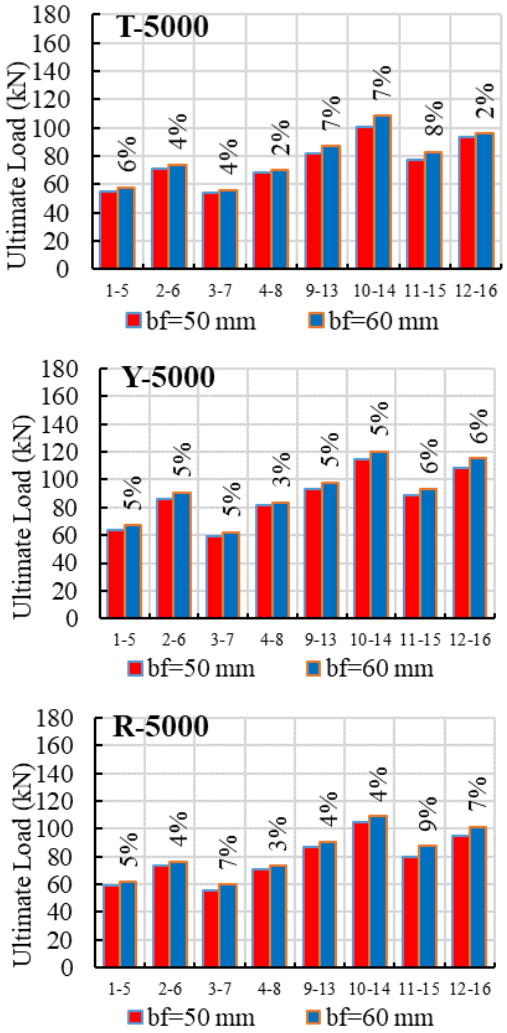

Figure 26: Difference in section load capacity between the beams with 50mm and 60mm in width.

4.7. Effect of changing steel beam depth

Increasing the depth has a significant impact on the total load of the specimen, as it can increase the load by about 50%, 45%, and 51% for T, Y, and R respectively for beams with a span of 4000mm, and the load increases by about 51%, 50%, and 47% for T, Y, R in respectively for beams with a span of 5000mm. Figure 27 shows a comparison between the beams with depths of 270mm and 370mm.

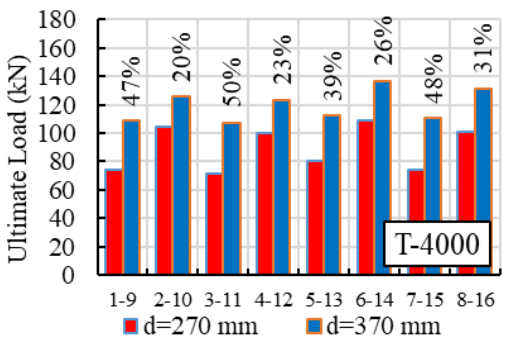

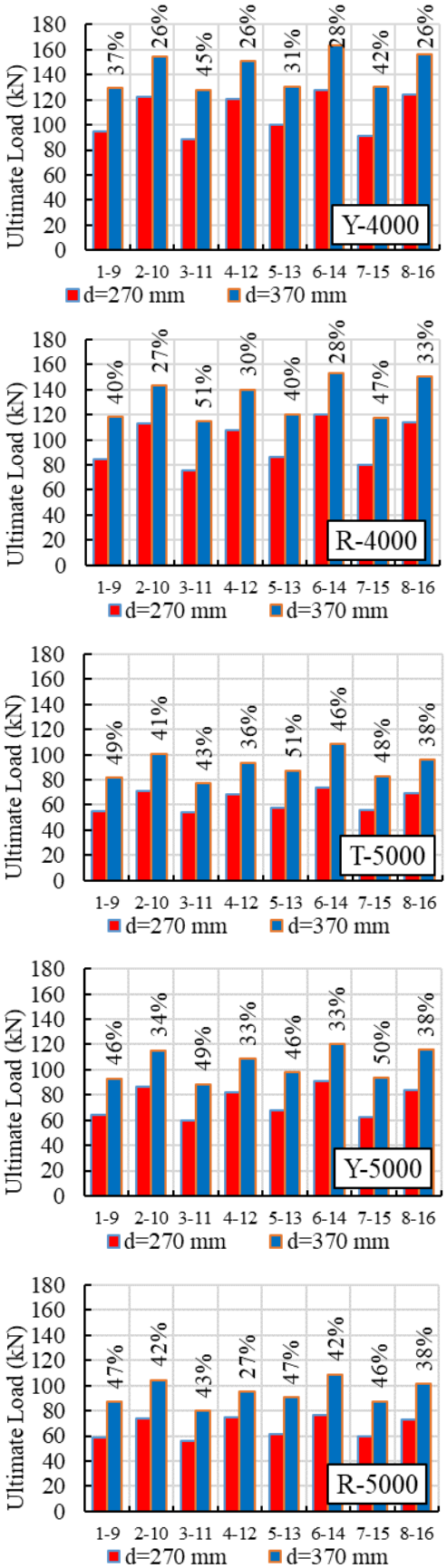

Figure 27: Difference in section load for beams with depths 270mm and 370mm.

4.8. Effect of Using Various Spans

Figure 28 shows a comparison between two simple spans versus load, it's found that the beam load capacity decreased in case of span 5000mm compared by span 4000 mm by about 32%, 33%, and 36% for T, Y, and R beams respectively.

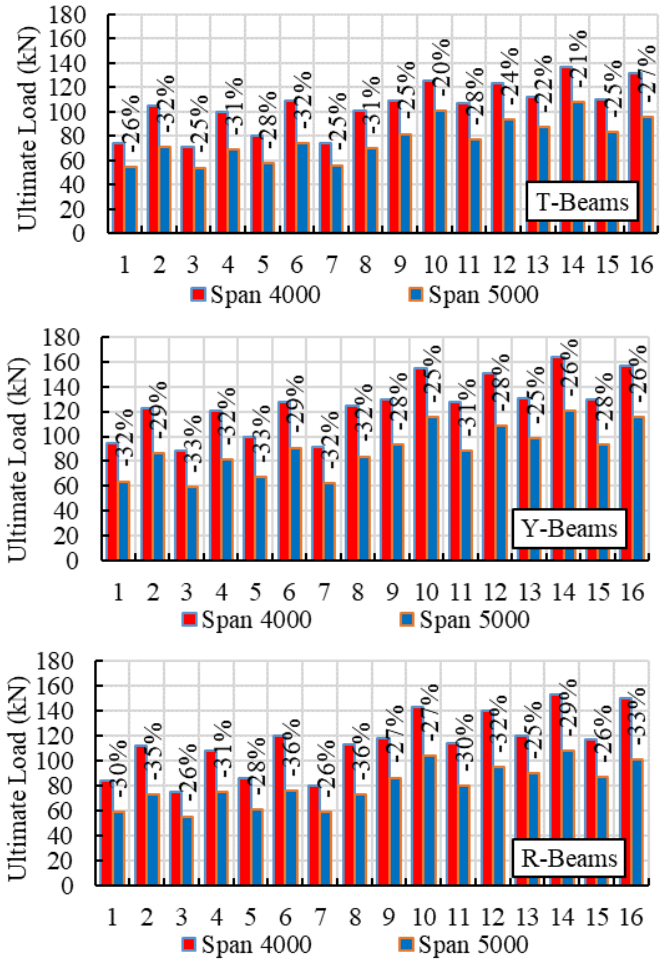

Figure 28: Difference in section load capacity for beams with spans of 4000mm and 5000mm.

5. CONCLUSIONS

The current research aimed to investigate the flexural behavior of composite CFS beams. Eight full-scale composite beam tests were verified using finite element software (ABAQUS). New parametric research was conducted to investigate new variables, including 96 models to evaluate factors such as beam cross-section shapes (T, Y, and R), beam lengths (4000mm, 5000mm), beam widths (50mm and 60mm), beam depths (270mm and 370mm), and slab thicknesses (50mm and 70mm). Based on the findings:

1- The verification findings indicated that the FEA results gives a good agreement with the Exp results.

2- In these types of beams, lateral buckling failure is regarded as the main mechanism of failure.

3- Beam cross section shape increases the section load capacity for beams with span 4000mm by about 28% for Y-sections and by about 14% for R-sections compared with the T-section results. Also increase the section load capacity for beams with span 5000mm by about 23% for Y-sections and by about 9% for R-sections.

4- Using web thickness=1.5mm and flange thickness =1.2mm decreases the section load capacity by about 10% for 4000mm beams and 11% for 5000mm beams than using flange thickness=1.5mm and web thickness=1.2mm.

5- Increasing the slab thickness from 50mm to 70mm increases the section load capacity by about 42% for beams with 4000mm and 38% for beams with 5000mm beams.

6- The effect of increasing the flange width from 50mm to 60mm on the section load capacity doesn't exceed 9%.

7- Changing beam depth from 270 to 370 enhances the section load capacity by about 51%.

8- Increasing the beam length from 4000mm to 5000mm decreases the section capacity by about 36%.

The resistance to lateral buckling may be marginally improved if web stiffeners were utilized across the span, while local buckling in the web might be reduced. By combining diaphragms with a double-T section, it is possible to further enhance the suggested cross-section and increase the steel components' resistance to lateral buckling.

However, the investigation's findings show that the flooring systems' functionality has improved. In order to provide structures with an alternative, lightweight floor system, it proposes an inventive floor system that combines built-up CFS sections with a concrete slab.

REFERENCES

[1] R.M. Lawson, Design of Composite Slabs and Beams with Steel Decking, the Steel, Construction Institute Publication, Berkshire, UK, 1989.

[2] D. Lam, Capacities of headed stud shear connectors in composite steel beams with precast hollow core slabs, J. Constr. Steel Res. 63 (9) (2007) 1160–1174.

[3] W.K. Yu, K.F. Chung, M.F. Wong, Analysis of bolted moment connections in cold-formed steel beam-column sub-frames, J. Constr. Steel Res. 61 (2005) 1332–1352.

[4] J.M. Irwan, A.H. Hanizah, I. Azmi, H.B. Koh, Large-scale test of symmetric cold-formed steel (CFS)–concrete composite beams with BTTST enhancement, J. Constr. Steel Res. 67(4) (2011) 720–726.

[5] Hanaor, Tests of composite beams with cold-formed sections, J. Constr. Steel Res. 54 (2000) 245–264.
[6] R.M. Lawson, S.O. Popo-Ola, D.N. Varley, Innovative development of light steel composites in buildings, in R. Eligehausen (Ed.), International Symposium on Connections between Steel and Concrete, Germany RILEM Publications SARL, Stuttgart, 2001.
[7] B.S. Lakkavalli, Y. Liu, Experimental study of composite steel C-section floor joists, J. Constr. Steel Res. 62 (2006) 995–1006.
[8] M.J. Irwan, A.H. Hanizah, I. Azmi, P. Bambang, H.B. Koh, M.G. Aruan, Shear transfer enhancement in precast cold-formed steel-concrete composite beams: effect of bent-up tabs types and angles. in: Proceedings of Technology and Innovation for Sustainable Development Conference (TISD2008), Faculty of Engineering, Khon Kaen University, Thailand, pp. 56–61.
[9] J.M. Irwan, A.H. Hanizah, I. Azmi, Test of shear transfer enhancement in symmetric cold-formed steel–concrete composite beams, J. Constr. Steel Res. 65 (2009) 2087–2098.
[10] Ahmed Kamar, Mahmoud Lasheen, et al., Factors affecting slip and stress distribution of concrete slabs in composite beams, Engineering Structures 245 (2021) 112880.
[11] T.M. Alhajri, M. M Tahir et al. Behavior of pre-cast U-shaped composite Beam integrating cold-formed steel with ferro-cement slab, Thin-Walled Structures 102 (2016) 18–29
[12] Y.C. Wong, Deflection of steel-concrete composite beams with partial shear interaction, J. Constr. Steel Res. 24 (10) (1998) 1159–1165.
[13] Ashraf M. Abou-Rayan, Nader N. Khalil, Ayman A. Zaky, Experimental investigation on the flexural behavior of steel cold-formed I-beam with strengthened hollow tubular flanges, Thin-Walled Structures 155 (2020) 106971
[14] J.Y. Richard, J.Y. Yiching, M.T. Lai, Composite beams subjected to static and fatigue loads, J. Struct. Eng. 123 (6) (1997) 765–771.
[15] A.E. Naaman, Ferrocement and Laminated Cementitious Composites, Techno Press 3000, Ann Arbor, Michigan, USA, 2000.
[16] Mohammad amin Azimi, Azlan Bin Adnan, Mahmood Md Tahir, Abdul Rahman Bin Mohd Sam, Sk. Muiz Bin Sk Abd Razak, Seismic performance of ductility classes medium RC beam-column connections with continuous rectangular spiral transverse reinforcements, Lat. Am. J. Solids Struct. 12(4)
[17] Talal, Structural Behavior of an Innovative Pre-cast Cold-formed Steel-Ferro-cement as Composite Beam, Thesis Doctor of Philosophy, University Teknologi, Malaysia, 2014.
[18] P.Avery, Mahen Mahendran, (1996), Finite Element Analysis of Hollow Flange Beams with Web Stiffeners, International Specialty Conference on Cold-Formed Steel Structures.
[19] Tarek Sharaf, Ashraf Elsabbagh, Mohamed Abdellatif, and Mohamed Elghandour, Flexural Behavior of Beams Fabricated Using Light Gauge Steel with Rectangular or Triangular Hollow Flanges Faculty of Engineering - Port Said University Volume 23 No. 1 March 2019 pp: 47:64.
[20] J. Leng, J. Yang, Z. Zhang, et al. Mechanical behavior of a novel compact steel-UHPC joint for hybrid girder bridges: Experimental and numerical investigation. Journal of Constructional Steel Research 2024, 218: 108742.
[21] Zhang Z, Pang K, Xu L, Zou Y, Yang J, Wang C. The bond properties between UHPC and stone under different interface treatment methods[J]. Construction and Building Materials, 2023. 365: 130092.
[22] Y. Zou, J. Jiang, J. Yang, et al. Enhancing the toughness of bonding interface in steel-UHPC composite structure through fiber bridging. Cement and Concrete Composites 2023, 137:104947.
[23] J. Yang, Flexural Behaviour of Ultra-High Performance Concrete Beams Prestressed with CFRP Tendons, 2007 [in Chinese.] Ph.D. dissertation Hunan.
[24] Z. Zhe, S.H.A.O. Xu-dong, L.I. Wen-Guang, Z.H.U. Ping, C.H.E.N. Hong, Axial tensile behaviour test of ultrahigh performance concrete, China J. Highway Transp. 28 (8) (2015) 50–58 (in Chinese).
[25] Tarek Sharaf, Mohamed Abdellatif, Mohamed Elghandour, Ashraf ElSabbagh, Experimental and finite element evaluations of single-T composite cold-formed steel beam with concrete slab, Engineering Structures 318 (2024) 118762.
[26] B.W. Schafer, T. Pekoz, (1998), Computational modeling of cold-formed steel: characterizing geometric imperfections and residual stresses, Journal of Constructional Steel Research, No. 47, pp. 193–210.
[27] Hong-Xia Wan, Mahen Mahendran, (2015), Bending and torsion of hollow flange channel beams, Engineering Structures No. 84, pp.300:312.